

# Lab on a Chip

Accepted Manuscript



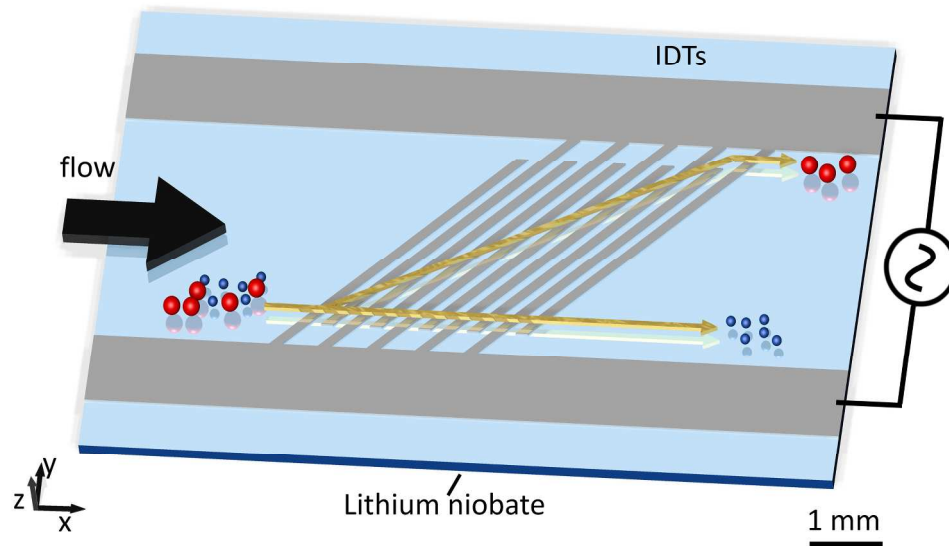
This is an *Accepted Manuscript*, which has been through the Royal Society of Chemistry peer review process and has been accepted for publication.

*Accepted Manuscripts* are published online shortly after acceptance, before technical editing, formatting and proof reading. Using this free service, authors can make their results available to the community, in citable form, before we publish the edited article. We will replace this *Accepted Manuscript* with the edited and formatted *Advance Article* as soon as it is available.

You can find more information about *Accepted Manuscripts* in the [Information for Authors](#).

Please note that technical editing may introduce minor changes to the text and/or graphics, which may alter content. The journal's standard [Terms & Conditions](#) and the [Ethical guidelines](#) still apply. In no event shall the Royal Society of Chemistry be held responsible for any errors or omissions in this *Accepted Manuscript* or any consequences arising from the use of any information it contains.

Sorting of particles measuring  $6.6\mu\text{m}$  and  $7.0\mu\text{m}$  has been achieved in a scheme in which lateral displacement is deterministic .



223x152mm (300 x 300 DPI)

# Particle separation using virtual deterministic lateral displacement (vDLD)

David J. Collins<sup>a</sup>, Tuncay Alan<sup>a</sup> and Adrian Neild<sup>\*a</sup>

Received Xth XXXXXXXXXXXX 20XX, Accepted Xth XXXXXXXXXXXX 20XX

First published on the web Xth XXXXXXXXXXXX 200X

DOI: 10.1039/b000000x

We present a method for sensitive and tunable particle sorting that we term virtual deterministic lateral displacement (vDLD). The vDLD system is composed of a set of interdigital transducers (IDTs) within a microfluidic chamber that produce a force field at an angle to the flow direction. Particles above a critical diameter, a function of the force induced by viscous drag and the force field, are displaced laterally along the minimum force potential lines, while smaller particles continue in the direction of the fluid flow without substantial perturbations. We demonstrate the effective separation of particles in a continuous-flow system with size sensitivity comparable or better than other previously reported microfluidic separation techniques. Separation of 5.0  $\mu\text{m}$  from 6.6  $\mu\text{m}$ , 6.6  $\mu\text{m}$  from 7.0  $\mu\text{m}$  and 300 nm from 500 nm particles are all achieved using the same device architecture. With the high sensitivity and flexibility vDLD affords we expect to find application in a wide variety of microfluidic platforms.

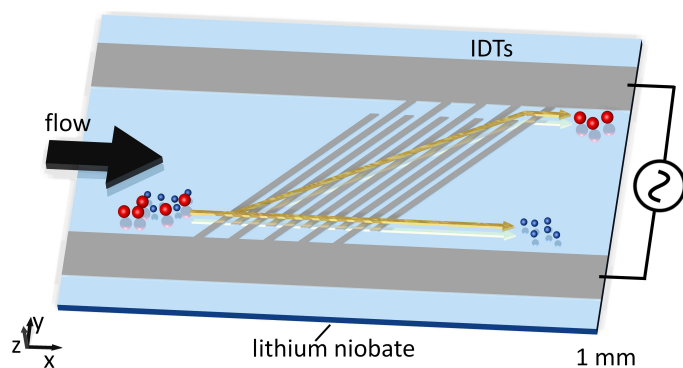


**Fig. 1** Sketch of the vDLD operating principle: a solution containing dissimilarly sized particles passes through an acoustic or electric field, created by an array of interdigital transducers (IDTs) on a piezoelectric lithium niobate (LN) substrate. Particles in the vDLD system are subject to both induced forces and viscous drag. Larger particles are captured in the force field and are transported laterally, while smaller particles are not significantly shifted.

## 1 Introduction

The separation of particles and cells is fundamental to a variety of chemical, biological and industrial processes<sup>1,2</sup>, where the concentration of a particular analyte is used to increase

diagnostic detection efficiency or therapeutic efficacy. Compared to conventional techniques, microfluidic systems can perform particle separation with less reagent, time and cost while taking advantage of forces that may be inapplicable on the macro-scales. Typically separation is enabled by the application of an external field, with efficiency determined by the differential effect the field has on particles with different properties. Microfluidic particle separation in continuous flow systems has been demonstrated using hydrodynamic<sup>3–5</sup>, magnetic<sup>6,7</sup>, optical<sup>8</sup>, dielectrophoretic (DEP)<sup>9–11</sup>, acoustic<sup>12,13</sup>, microfabricated electrophoretic arrays<sup>14–16</sup> and passive mechanical methods, including brownian ratchets<sup>17,18</sup> and deterministic lateral displacement (DLD)<sup>19–23</sup>, with each of these techniques having different advantages and operating ranges in terms of allowable sizes, sample types and throughput.

A DLD system consists of a microfluidic channel containing a periodic array of pillars such that each subsequent row is offset in the lateral direction. This broken symmetry results in multiple streamlines that co-exist within the channel. Particles with a diameter smaller than a critical value travel with the forward flow, while larger particles are "bumped" sideways<sup>20,25</sup>. In addition to their sensitivity, DLD devices have the additional advantage of being a passive system without pre-treatment requirements. However, as separation depends on the geometric distribution of the pillars, individual devices must be fabricated to suit specific particle size ranges. Similarly, any structural irregularities affect the flow profile (due to the number of pillars there is a large number of sites for potential defects), possibly resulting in stiction and blockages. Moreover, relatively long channel lengths are required to achieve significant lateral displacement.

† Electronic Supplementary Information (ESI) available: video of particle separation (Video 1). See DOI: 10.1039/b000000x/

<sup>a</sup> Laboratory for Micro Systems, Department of Mechanical and Aerospace Engineering, Monash University, Clayton, VIC 3800, Australia. \*Tel: +61 3 990 54655; E-mail: [adrian.neild@monash.edu](mailto:adrian.neild@monash.edu)

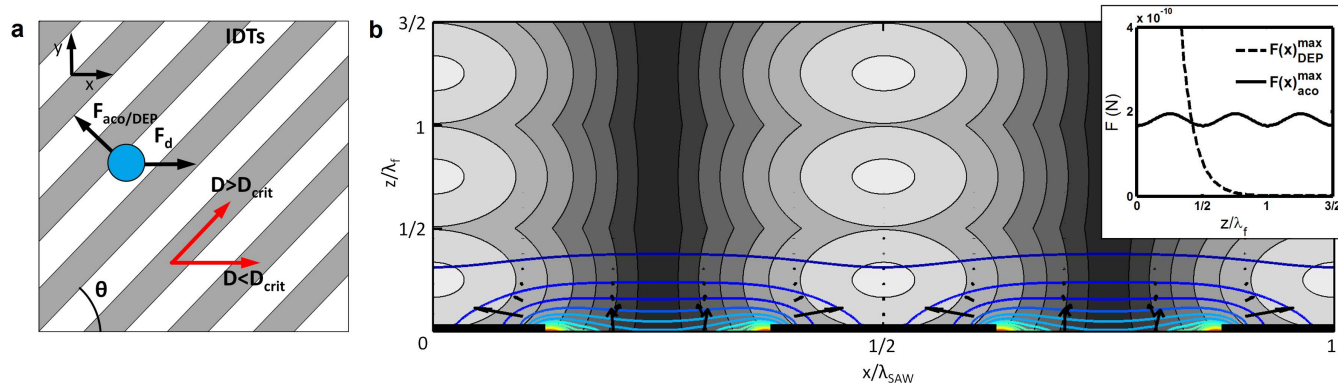


**Fig. 2** (a) A particle in the vDLD system is subject to forces of viscous drag  $F_D$ , the acoustic force  $F_{aco}$  and/or the DEP force  $F_{DEP}$ . The predominant force, DEP or acoustic, acting on a particle is determined by its distance above the IDTs. (b) Shows the acoustic pressure field magnitude in gray, the first 10 DEP force potential contours in color and the linearly scaled DEP force vectors in relation to the position of the IDTs (black). For representative values of voltage and pressures ( $\sim 5$  V,  $\sim 100$  kPa) that are generated on a piezoelectric such as lithium niobate at frequencies on the order of 10's of MHz on polystyrene particles in water, the maximum acoustic force in the  $x$ -direction  $F(x)_{aco}^{max}$  is dominant for heights greater than approximately half of the acoustic wavelength in the fluid  $\lambda_f$  (inset). The DEP force contours were derived from the method in Morgan et al, 2001<sup>24</sup>.

Here we address these issues by replacing the DLD pillar array with virtual obstacles, combining the principles of DLD with the flexibility of modifiable acoustic and DEP forces. Both acoustic and electric fields act differentially on particles and cells placed within them according to their size and mechanical or electrical properties, translating particles with impressive rapidity<sup>26</sup>.

Using acoustic forces it is possible to sort based on stiffness and density, with certain particles migrating to pressure antinodes and others to the pressure nodes<sup>13</sup>, and is in this sense a deterministic method, though this is only possible in the case where two particle populations have opposite-signed acoustic contrast factors. However, in sorting based on particle size, the fundamental principle of acoustic methods that have been shown to date is based on the size-dependant speed of particle migration in a uniformly applied field; hence sorting is a temporal rather than deterministic effect.

Destgeer et. al recently demonstrated a particle separation device using traveling surface acoustic waves (SAW)<sup>27</sup>; SAW is an acoustic actuation method that is especially applicable to microfluidic systems with the ability to easily localize and direct acoustic energy with wavelengths on the order of microfluidic systems (5-300  $\mu\text{m}$ ). Here, SAW was used to create a traveling wave acoustic field whose interfacial force scales with particle radius with  $F_{tw} \sim R^6$ . Alternatively, particle separation can be performed using standing waves, with  $F_{sw} \sim R^3$ ; when an acoustic field is generated in a half wavelength standing wave resonating channel it is possible to move particles from antinodal to nodal positions<sup>12</sup>, though this design is limited in its separation sensitivity due to the short distance ( $1/4\lambda$ )

over which particles are separated. In both cases the particle size differences reported are limited to  $\sim 300\%$ , despite the impressive acoustic force scalings. It has not been possible to sort particles deterministically – with particles above or below some critical diameter moving in different directions – in systems where these force scalings are simply applied directly.

Sorting is also possible using DEP, imparting a differential force on particles and cells based on their size and electrical properties. Park et al. used an array of electrodes patterned on a glass slide at an angle to the flow direction to sort particles and cells, separating 1  $\mu\text{m}$  from 10  $\mu\text{m}$  particles and *E. coli* from whole blood<sup>10</sup>. The separation demonstrated here was not deterministic, however, which would require a sharp cutoff between particles with only fractionally different properties, sending particles with particular values in a specific direction without significantly affecting the trajectory of other particles, rather than sorting particles on the basis of a parameter gradient.

To improve on the capabilities of microfluidics for particle separation, we have developed a novel SAW-based dynamically tunable particle sorting method with excellent separation efficiencies. This method makes use of acoustic forces or DEP, where the predominance of either force is determined by the channel dimensions. Particle separation in vDLD is *deterministic* in that particles above a critical size will be sorted from smaller ones, and *virtual* in that the acoustic/electric field – the fundamental equivalent of pillars in a DLD array – is non-material and can be adjusted to suit a given size range. Because the separation of particles for given sizes is determined only by the frequency, voltage/pressure amplitude and

flow rate, it is possible to separate particles over a wide size range, from nanometers to micrometers. Importantly, the ability to choose the dominant force permits sorting based on different particle/cell properties; acoustic forces permit sorting based on mechanical properties (compressibility, density), while DEP allows sorting based on electrical properties (permittivity).

The virtual deterministic lateral displacement (vDLD) system employs high frequency SAW and is depicted in Fig. 1. This method is not inherently limited to any particle size range. Importantly, we show that separation with only fractional differences in particle sizes is possible, with the effective separation of  $5.0 \mu\text{m}/6.6 \mu\text{m}$ ,  $6.6 \mu\text{m}/7.0 \mu\text{m}$  and  $300 \text{ nm}/500 \text{ nm}$  particles, all using the same device. Additionally, we show that this sorting is possible using two distinct forces with the force relevant for sorting dictated by the channel dimensions.

## System principles

The vDLD system is comprised of a microfluidic channel aligned on top of a high-frequency SAW device, composed of a series of aluminium interdigital transducers (IDTs) arrayed on a piezoelectric lithium niobate (LN) substrate. When an A/C signal is applied across the IDTs at a resonant frequency  $f = c_s/\lambda_{\text{SAW}}$ , where  $c_s$  is the sound speed in the substrate and  $\lambda_{\text{SAW}}$  is the spacing between successive IDT finger-pairs, the surface displacements emanating from a finger-pair are reinforced by those of nearby finger-pairs. As a result both an acoustic and an electrical field are created in the vicinity of IDTs, as seen in Fig. 2, either of which can be used for sorting. Moreover, both can be used for *deterministic* sorting; in the case of the size parameter, as long as there exists some critical diameter  $D_{\text{crit}}$  above which particles are trapped in a force field and below which they are not, it is possible to have a sharp cutoff in the lateral displacement of particle sizes. Here we discuss these forces, acoustic and dielectrophoretic, followed by how each determines  $D_{\text{crit}}$ .

A particle immersed in a standing wave pressure field experiences a maximum time averaged force given by<sup>12</sup>

$$F_{\text{aco}}^{\text{max}} = - \left( \frac{\pi P^2 V_p \beta_f}{2\lambda} \right) \phi, \quad (1)$$

where

$$\phi = \frac{5\rho_p - 2\rho_f}{2\rho_p + \rho_f} - \frac{\beta_p}{\beta_f}, \quad (2)$$

$V_p$  is the particle volume,  $\lambda$  is the wavelength,  $\rho_f$  and  $\rho_p$  the density of the fluid and particles,  $\mu$  the viscosity,  $\beta_p$  and  $\beta_f$  are the compressibility of the particle and medium and  $P$  is the acoustic pressure amplitude. In the case of a finite number

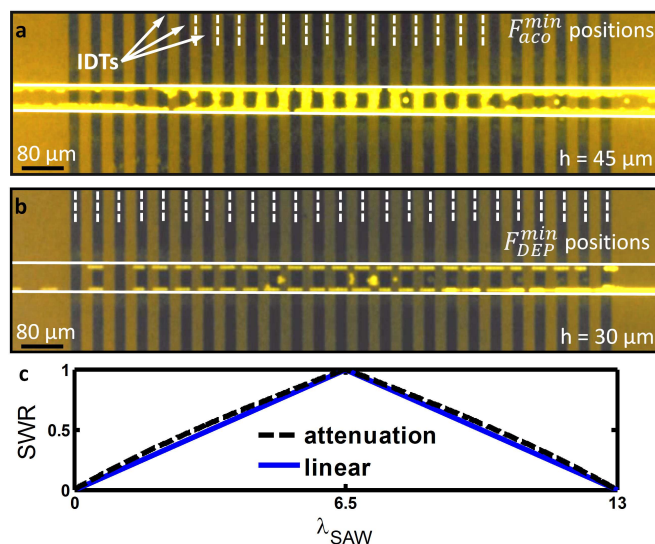


**Fig. 3** The height of the microfluidic chamber will determine which force,  $F_{\text{DEP}}$  or  $F_{\text{aco}}$ , predominates. (a) The acoustic field is the dominant force above the transducers for larger channel heights, with particle (here with a diameter of  $6.6 \mu\text{m}$ ) accumulation at the acoustic nodal positions between the IDTs. (b) Lowering the chamber height increases the horizontal component of the DEP force that can act on the particles, with particles observed to align directly above the transducers, and reduces the relative influence of the acoustic force as evidenced by the smaller number of acoustic nodes that contain particles. Particles are pushed to the edge of the channel due to the acoustic force maximum in the channel center – PDMS at the channel edges attenuates the surface displacements driving the acoustic force – and the flow condition through the channel ( $0.5 \mu\text{l}/\text{min}$ ). (c) In an acoustic field generated by a finite number of transducers the standing wave ratio (SWR) will vary across the length of the IDTs, modeled as the summation of acoustic displacements from neighboring finger pairs, shown here including and excluding the attenuation of a SAW under water (here with a decay length of  $9.24 \lambda_{\text{SAW}}$ <sup>28</sup>).

of finger-pairs, the pressure amplitude varies across the length of the IDT finger-pairs (Fig. 3(a,c)).

As a by-product of exciting the acoustic field, an electrical field between the IDTs finger pairs is produced as well, though this field is not explicitly required for sorting. A particle immersed in this electrical field will be subject to a time-averaged dielectrophoretic (DEP) force determined by that particles frequency-dependent polarisability relative to the medium, given by

$$F_{\text{DEP}} = 2\pi\epsilon_m R^3 \text{Re}(K) \nabla |E_{\text{rms}}|^2, \quad (3)$$

where  $\epsilon_m$  is the permittivity of the media,  $K$  is the Clausius-Mossotti factor dependent on the relative permittivity of the particle and media, varying between  $-0.5$  and  $1$ , and  $E_{\text{rms}}$  is

the root-mean-square electric field<sup>29</sup>. The acoustic and DEP force fields have been modeled and are shown in their relation to the interdigital transducers and how they evolve vertically from the substrate surface in Fig. 2. Generally speaking, DEP is only relevant in the vicinity of the electrodes, with the force magnitude dropping off exponentially from the substrate surface. In the direction that is relevant to sorting – the  $x$ -direction – the acoustic force is dominant for  $h \gtrsim 1/2\lambda_f$  (Fig. 2b). Each force will locate particles to different positions in the vDLD array. For a negative  $Re(K)$  value, particles will be vertically repelled and shifted horizontally to locations directly above the IDTs, as shown in Fig. 3b. In contrast, acoustic forces will shift particles to locations of minimum pressure, located between transducers, shown in Fig. 3a. Because DEP pushes particles with a negative  $Re(K)$  vertically, the height of the chamber therefore determines which force will be useful for sorting. Regardless of which force this is, the same fundamental behavior is expected because the force in both cases scales with  $F \sim R^3$  and its periodic variation with the IDTs. A particle under the influence of either of these forces is also subject to a viscous drag force  $F_D$ , given by

$$F_D = -6\pi\mu R u, \quad (4)$$

where  $\mu$  is the fluid viscosity,  $R$  is the particle radius,  $u$  is the differential velocity between particle and fluid and  $F_D^{max} = -6\pi\mu R v_f$  represents the maximum drag possible, where  $u$  is replaced by the fluid velocity  $v_f$ . Here, particle separation occurs because of the different scaling of acoustic/DEP and drag forces, with  $F_{aco/DEP} \sim R^3$  and  $F_D \sim R$ . The ability of a particle to pass through an acoustic/DEP force field will be determined by the maximum of each of these forces that are generated, as shown in Fig. 2a (a cross section in the  $x$ - $y$  plane).

In the case of the acoustic force, equating equations 1 and 4 where  $u = v_f$ , we find the critical particle diameter  $D_{crit}^{aco}$  at which the maximum acoustic force will equal the maximum drag force; a particle traveling orthogonally to an acoustic field in a continuous flow with dimensions larger than  $D_{crit}^{aco}$  will be trapped at any node/antinode, depending on the acoustic contrast factor  $\phi$ . For most particles and cells, however,  $\phi$  is positive, resulting in particle migration to acoustic nodes. Accounting for an acoustic field at an angle  $\theta$  to the flow field,  $D_{crit}^{aco}$  is found to be

$$D_{crit}^{aco} = 2 \cos^2(\theta) \sqrt{\frac{9\mu\lambda v_f}{\pi\beta_f P^2 \phi}}. \quad (5)$$

Similarly, the critical diameter for a particle immersed in a DEP force field can be found by equating equations 3 and 4, with

$$D_{crit}^{DEP} = 2 \cos^2(\theta) \sqrt{\frac{-3\mu v_f}{\epsilon_m Re(K) \nabla |E_{rms}|^2}}, \quad (6)$$

valid for negative values of  $Re(K)$ .

Here,  $\theta$  is chosen based on qualitative design and performance considerations. A large  $\theta$  will displace particles by large lateral distances, but will have a larger  $D_{crit}$  than a small  $\theta$  value, which conversely will be able to sort smaller particles, though with less lateral displacement.

The presence of a critical diameter, above which particles become trapped and below which they do not, is the basis for deterministic sorting, with trapped particles exiting the force field at a different location to non-trapped particles. However, this will only occur when the particles all experience a similar  $v_f$  value. Though the IDTs are oriented in the  $x$ - $y$  plane, the field that is generated varies vertically as well<sup>30</sup>; for this we examine the pressure and velocity field in the  $x$ - $z$  plane. Two chamber heights were tested experimentally: one with  $h = 1/2\lambda_f$  and a second with  $h = 3/2\lambda_f$ . In the case of a chamber with a height such that the DEP force dominates ( $h = 1/2\lambda_f$ ), this is readily realized in that particles will be repelled to the chamber roof. However, in the case where acoustic force determines the particle trajectory, the particles will follow paths where they experience minimal acoustic forces. For example, with a chamber height  $h = 3/2\lambda_f$ , this occurs at  $h = \lambda_f$ ; the finite size of particles means that the acoustic force will be greater at the chamber roof, and a repellant DEP force prevents particles taking a path across the IDTs at  $h = 1/2\lambda_f$ . These effects have been observed experimentally: randomly distributed particles immersed in a horizontal flow will slow down as they are pushed into slower-moving flow at the chamber roof when  $h = 1/2\lambda_f$ , and can be seen to (on average) speed up when  $h = 3/2\lambda_f$  as they are pushed into faster moving flow in near the middle of the parabolic flow profile in the  $z$ -direction.

Any chamber with height  $h \lesssim 3/2\lambda$  will result in all particles of the same diameter experiencing the same local forces. Acoustic nodes/antinodes will still be formed for larger chamber heights, however this would reduce the possibility for reliable deterministic displacement due to multiple possible particle trajectories in the  $z$ -direction, each with a unique  $v_f$ ,  $F_D^{max}$  and  $F_{aco/DEP}^{max}$ .

With the criteria established with regard to the height dimensions, attention can be returned to the  $x$ - $y$  plane, as this is the plane in which sorting occurs. Fig. 4 and Fig. 5 show the deterministic sorting of micro and nano-scale particles, respectively; particles with diameters  $D < D_{crit}$  (blue) are able to proceed with minimal lateral displacement, albeit more slowly than the fluid velocity. In contrast, particles above a critical diameter  $D_{crit}$ , occurring when the particle velocity that is induced by the acoustic/DEP force is greater than that of the local fluid velocity, will not be able to pass across a force maximum. It is important to note that the local fluid velocity  $v_f$  will vary in the  $y$ -direction due to the fully developed laminar flow profile. At the start of the chamber (left), with

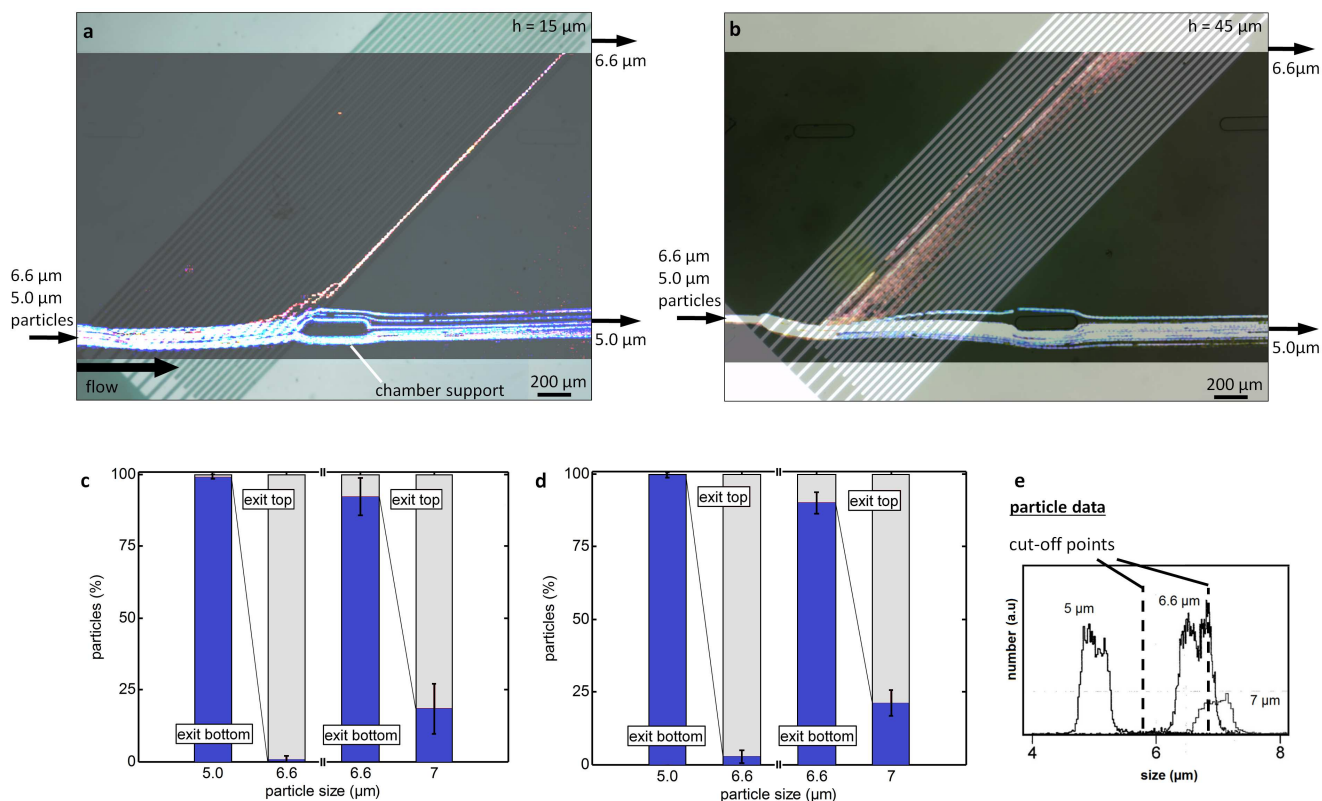


**Fig. 4** vDLD particle sorting is possible in devices where either DEP or acoustic forces determine particle trajectory, with captured particles translating on top of the IDTs in the case of DEP and between them in the case of the acoustic force. (a) Maximum intensity plot of fluorescent particles overlaid on a brightfield image of a device with height  $h = 15 \mu\text{m}$  and peak-to-peak voltage of 4 V, where a solution of blue  $5.0 \mu\text{m}$  orange  $6.6 \mu\text{m}$  particles passes through a truncated vDLD array with 13 finger-pairs, angled at  $\theta \approx 45^\circ$  to the flow direction, with particles of diameters  $D > D_{crit}$  being laterally separated from particles with  $D < D_{crit}$ . The same is shown for a device in which acoustic forces are expected to dominate in (b), with  $h = 45 \mu\text{m}$  and applied power of  $0.0781 \text{ W/mm}^2$ , as evidenced by the capture of particles along acoustic nodes in the region of the IDTs where the acoustic force is at a maximum (see Fig. 3). The effectiveness of both forces for particle separation is evidenced by their comparable sorting efficiencies. (c,d) Shows the the respective separation efficiencies of two particle population sets ( $[5.0 \mu\text{m}, 6.6 \mu\text{m}]$  and  $[6.6 \mu\text{m}, 7.0 \mu\text{m}]$ ) for devices where  $h = 15 \mu\text{m}$  (c) and  $h = 45 \mu\text{m}$  (d). Separation efficiency of the particle populations is limited by the existing overlap in their size distributions, given in (e), obtained from the particle manufacturer (Magsphere Inc, Pasadena, CA). Flow rates in both cases are  $4.1 \mu\text{l/min}$  with a SAW wavelength of  $80 \mu\text{m}$ .

this condition not being met, the larger particles cross from one IDT pair to the next, though are still slightly retarded and laterally shifted. By designing the device such that the particles are introduced into the center of a channel with buffer fluid making up the volume on either side, each lateral displacement in the resulting parabolic velocity field moves the particles into slower flowing fluid so that the acoustic force becomes increasingly dominant, corresponding to increasing lateral shifts. Eventually the fluid flow is reduced such that  $F_{aco}^{max}/DEP \geq F_D$ ; for optimum sorting this condition should occur at the last possible acoustic pressure antinode or DEP force maximum. In the case of an acoustically generated force and a finite set of IDTs, it should be noted that this antinode will

occur near the middle of the IDT array (see Fig. 3).

Critical to acoustic deterministic sorting is the ability to control the topographical amplitude of the acoustic field, namely to maintain a relatively constant surface displacement across the width of the IDT aperture. By acting on particles as they pass over the IDTs themselves, in contrast to systems where the IDTs generate an acoustic field outside of the fluid-covered region<sup>31,32</sup>, the amplitude variance across the aperture width that occurs in far field SAW can be avoided<sup>33,34</sup>, while simultaneously eliminating what would otherwise be the significant SAW amplitude attenuation at the LN-PDMS interface<sup>35</sup>.

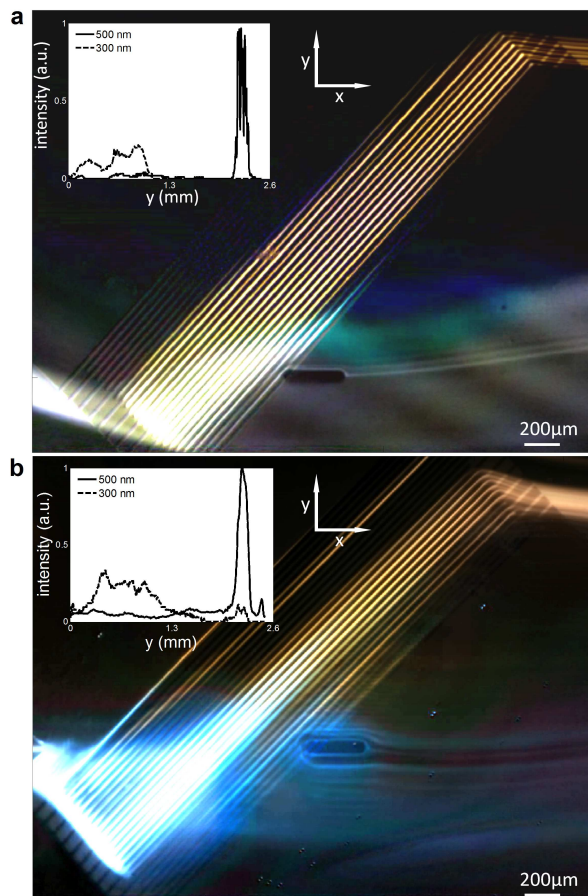


**Fig. 5** (a,b) shows average intensity images with separation of fluorescent blue 300 nm and 500 nm orange ( $\sigma_{300} = 39$  nm,  $\sigma_{500} = 16$  nm) particles passing through a vDLD device with (a)  $h = 15$   $\mu\text{m}$  [3.8 V, 0.45  $\mu\text{l}/\text{min}$ ,  $\lambda_{SAW} = 80$   $\mu\text{m}$ ] and (b)  $h = 45$   $\mu\text{m}$  [0.369  $\text{W}/\text{mm}^2$ , 1.8  $\mu\text{l}/\text{min}$ ,  $\lambda_{SAW} = 80$   $\mu\text{m}$ ]. 500 nm particles are observed to travel at an angle to the flow in the direction dictated by the force field. 300 nm particles subjected to the same force field experience a smaller induced force, with their trajectory determined instead by viscous drag. Insets show intensity plots of fluorescent particles with background subtracted; approximately 87% [in (a)] and 79% [in (b)] of 500 nm particles, as measured by the integral of the intensity profiles, are separated from the 300 nm particles.

## Methods

The vDLD device here consists of a 13 finger pair 80  $\mu\text{m}$  wavelength set of 5/250 nm chrome/aluminium IDTs arrayed on a 0.5 mm thick, double side polished  $128^\circ$   $Y$ -cut,  $X$ -propagating LN substrate operating at 49 MHz. To insulate the transducers, prevent corrosion and promote adhesion with the polydimethylsiloxane (PDMS) chamber, the SAW device was coated with 200 nm of  $\text{SiO}_2$ . The PDMS (1:5 ratio of curing agent/polymer) chamber, with height 15  $\mu\text{m}$  or 45  $\mu\text{m}$ , was bonded with the device after exposure to an air plasma (Harrick Plasma PDC-32G, Ithaca, NY, 1000mTorr, 18W). Polystyrene particles (Magsphere, Pasadena, CA, USA) enter the laterally symmetric 5 mm wide chamber through a 20  $\mu\text{m}$  particle injection port. Due to the high aspect ratio (up to 300:1), 200  $\mu\text{m}$  wide chamber supports were periodically spaced to prevent collapse and maintain chamber height. The buffer solution consisted of deionized water (Miili-Q 18.2  $\text{M}\Omega\cdot\text{cm}$ , Millipore, Billerica, MA) with 0.2% polyethylene glycol to prevent particle adhesion. Experiments were visualized using a fluorescent microscope (Olympus BX43, Tokyo, Japan) and imaged using a 5MP C-mount camera (Dino-Lite AM7023CT, New Taipei City, Taiwan). In order to demonstrate system versatility, all experiments were performed using the same device. The pressure amplitude was determined by  $P = v_s \rho c_f$ , where  $v_s$  is the substrate velocity, determined using a laser Doppler vibrometer (LDV, UHF-120; Polytech GmbH, Waldbronn, Germany).

## Results and Discussion

Fig. 4 shows the sorting of 5.0  $\mu\text{m}$  and 6.6  $\mu\text{m}$  particles (green and orange in Supplementary Video 1), which enter the vDLD array at the middle of the chamber. In both In Fig. 4(a,b), the applied voltage/power and flow rate have been specifically tuned to place the larger 6.6  $\mu\text{m}$  particles in the last few possible force minima for most effective sorting. As discussed previously and shown in Fig. 3, this is located near the middle of the IDT array for the case where the acoustic pressure determines the particle trajectory ( $h = 45$   $\mu\text{m}$ ) and at the end of the array when DEP is dominant ( $h = 15$   $\mu\text{m}$ ). During the experiment the particles were counted individually, with  $99.1 \pm 0.7\%$  and  $99.3 \pm 1.3\%$  of each particle size range successfully separated in the DEP-dominant case, and  $99.5 \pm 0.5\%$  and  $97.3 \pm 2.7\%$  in the acoustically-dominant one, where larger 6.6  $\mu\text{m}$  particles exit the pressure field separated by the vertical span of the IDTs. Particle separation efficiency is marginally reduced to 80–90% when sorting between 6.6  $\mu\text{m}$  and 7.0  $\mu\text{m}$  particles (less than 6% size difference). However, for both of the particle size ranges separated in Fig. 4 the quantity of unsorted particles, i.e those observed to follow an unintended trajectory, is on the same order of the

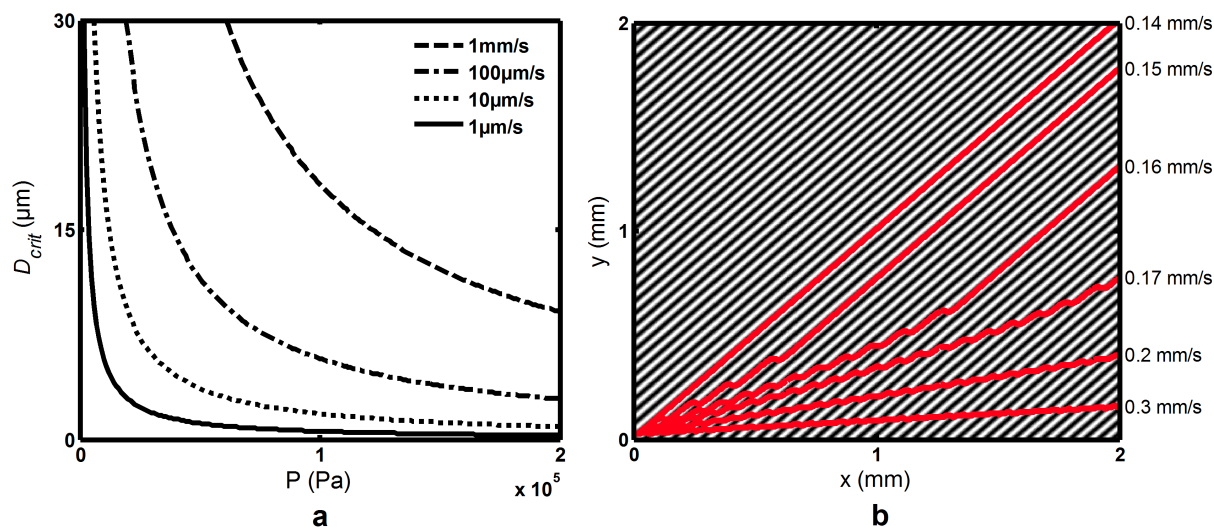


**Fig. 6** The critical particle diameter  $D_{crit}$  for a given acoustic antinode is a function of the local fluid velocity and pressure amplitude. (a) Shows the relationship between  $D_{crit}$  and pressure amplitude for various realizable microfluidic flow rates when the acoustic field is angled at  $45^\circ$  to the fluid flow. Here, different values for pressure amplitude and flow velocity were inserted into Eq. 5. The existence of multiple IDT pairs spanning a laterally oriented parabolic velocity field in the vDLD system, however, means that higher flow rates can be used than might be inferred from (a). In (b), a polystyrene  $10 \mu\text{m}$  particle in a 49 MHz 100kPa pressure field will eventually be trapped in an acoustic node, regardless of the flow rate, provided the acoustic field is sufficiently elongated horizontally. Flow velocity is at a maximum at the site of particle injection, parabolically decreasing with increasing lateral distance.

value of overlap in the particle size distribution (Fig. 4e). Increasing voltage/SAW-amplitude or decreasing flow velocity would cause the larger particles to follow a pressure node encountered earlier, decreasing the sensitivity of the device to the particular size range tested here.

A major advantage of the vDLD system is that particles over a large size range can be similarly separated, requiring only a change of flow rate and amplitude. Using the same devices used to separate micron-sized particles in Fig. 4, we demonstrate the separation of sub-micron particles, showing the viable separation of 300 nm and 500 nm particles (blue and orange, respectively) in Fig. 5. Here, separation efficiency in Fig. 5(insets) is determined by the normalized image intensity of the final ten rows of pixels in the x-direction, rather than particle counting, as the particles could not be visualized individually. The separation of these small particles is made possible by the relatively high frequency used to do so. For a given frequency of actuation, there exists a particle size below which acoustic streaming, rather than though acoustic pressure field, dictates particle motion. This diameter is given by  $d_c = \delta \sqrt{6\Psi/\phi}$ , where  $\Psi$  is a geometry dependent factor (0.375 for a standing wave in a flat-walled chamber),  $\phi$  is the acoustic contrast factor from Eq. 2 and  $\delta = \sqrt{2\mu/\rho\omega}$ , the acoustic boundary layer thickness<sup>36</sup>. At a frequency of 50 MHz, for example, it should be theoretically possible to cap-

ture particles as small as 200 nm in an acoustic standing wave in water.

To better understand the parameters (velocity, pressure and diameter) that determine particle displacement, the vDLD system was modeled. To avoid duplication, the force field is modeled here as being acoustically generated. The analysis presented here, however, could easily be extended to a DEP-dominated particle trajectory.

The particle velocity  $\mathbf{u}$  is determined by the contributions resulting from the acoustic field,  $u_{F_{aco}}$ , and that of the parabolic fluid velocity field  $v_f$ , given by

$$\mathbf{u} = \nabla (u_{F_{aco}}^{max} k (x \cos(\theta) + y \sin(\theta))) + v_f(y), \quad (7)$$

where  $u_{F_{aco}}^{max}$  is the maximum migration velocity that can be induced by the acoustic field alone,  $k = 2\pi/f$  is the wavenumber,  $(x, y)$  denotes the horizontal and vertical spatial coordinates, and

$$u_{F_{aco}}^{max} = \frac{F_{aco}^{max}}{6\pi\mu R}, \quad (8)$$

with  $v_f$  determined by

$$v_f = v_f^{max} (1 - y^2/y^{max}). \quad (9)$$

This velocity field was simulated using the MATLAB function *streamline*, with simulated particles subject to various

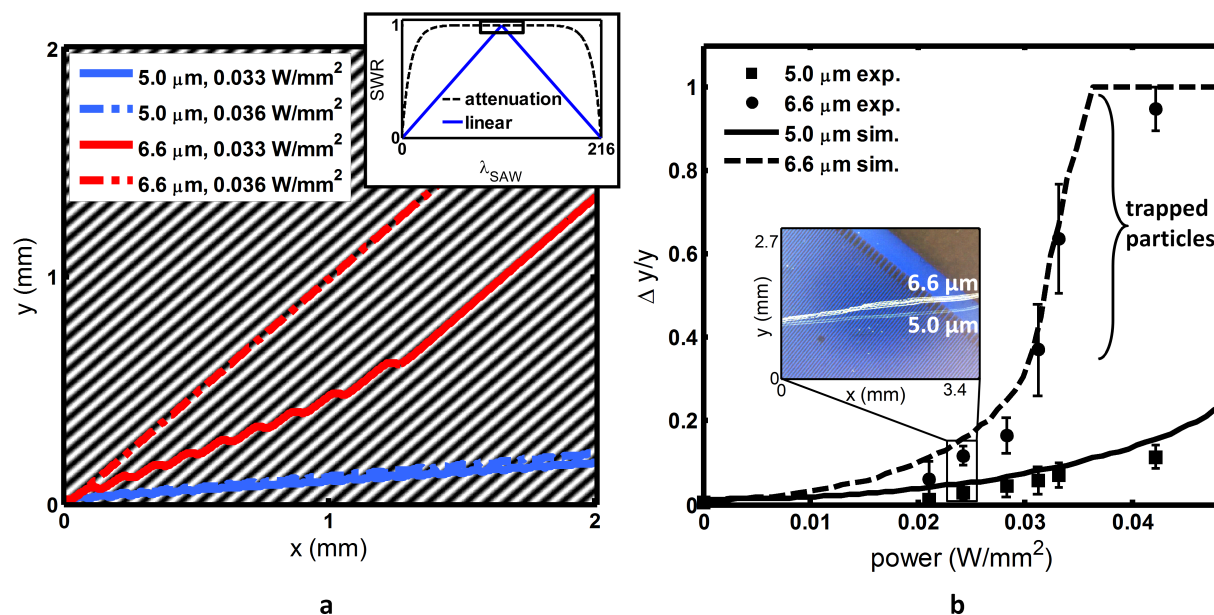


**Fig. 7** In a continuous force field the lateral displacement is a function of particle size and applied power. (a) shows the particle path traced through an acoustic force field for different particle sizes and energy densities. When a particle is close in size to  $D_{crit}$ , even a small change in parameters can have a large influence in that particles lateral displacement. A large enough number of IDTs yields a spatially uniform acoustic field (inset), as simulated here. (b) In a separate set of experiments, 5.0  $\mu\text{m}$  and 6.6  $\mu\text{m}$  particles were introduced into a continuous acoustic field [ $\lambda_{\text{SAW}} = 100 \mu\text{m}$ , 39 MHz device with 216 finger pairs,  $h \approx 50 \mu\text{m}$ ] with the same flow conditions (4.1  $\mu\text{l/s}$ ,  $v_f^{max} = 0.35 \text{ mm/s}$ ) as simulated in (a) and compared against these simulation results, with the inset showing representative maximum intensity images of 5.0  $\mu\text{m}$  (green) and 6.6  $\mu\text{m}$  (orange) particles across the continuous IDT array. Higher powers yield larger separation distances. The pressure field is determined by  $P = v_s \rho c_f$ , where the substrate velocity  $v_s$  was measured using a laser doppler vibrometer. For 6.6  $\mu\text{m}$  particles, displacement plateaus for power densities greater than approximately 0.035  $\text{W}/\text{mm}^2$ , though these particles are essentially trapped in an acoustic node by the end of the test area for power densities approximately greater than 0.03  $\text{W}/\text{mm}^2$ . Here error bars show the spatial extent of observed particles and experimental points show the midpoint of this observed displacement.

flow rates and pressures. Fig. 6a shows the relationship between  $D_{crit}$  and pressure amplitude. As per Eq. 5,  $D_{crit}^{aco} \sim v_f^{0.5}/P$ , with lower fluid velocities yielding a smaller  $D_{crit}^{aco}$ . With multiple IDT pairs, however, it is possible to displace particles of a given size for higher maximum flow rates more than would be suggested by Fig. 6a. Each successive antinode will shift a given particle laterally, where each shift moves the particle into a lower local fluid velocity in a parabolic laminar flow profile. Fig. 6b shows that, provided the spatial extent of the pressure field is sufficiently large, multiple flow rates will lead to eventual particle capture when a particle is sufficiently laterally shifted such that  $F_{aco}^{max} \geq F_D$  locally. Here, maximum flow velocities  $v_f^{max} \lesssim 0.17 \text{ mm/s}$  result in particle capture within 2 mm for the pressure conditions given. Similarly, a particle of any size will eventually be captured in an acoustic node in such a field for given flow velocity and pressure amplitude conditions, allowing particles to be sorted in a definable gradation. This modeling approach is validated by comparing the simulation results with experimental results

in a continuous acoustic field. Fig. 7a shows the influence a relatively small change in applied power density (with pressure amplitude  $P = v_s \rho c_f$ ) will have on lateral displacement. This is also observed experimentally in Fig. 7b, with sharp increases in 6.6  $\mu\text{m}$  particle displacement for power densities  $\gtrsim 0.03 \text{ W}/\text{mm}^2$ . In both cases the acoustic field was modeled here as being locally uniform; if the number of IDTs creating the acoustic field is sufficiently large, the attenuation of SAW under water means that the field strength will vary by less than 0.05% in the central half of a field created by 216 finger pairs.

For more *deterministic* sorting, however, with greater lateral separation between particles on either side of a given diameter, it is practical to limit the number of finger pairs used. In doing so, the final acoustic antinode encountered determines the  $D_{crit}^{aco}$  of the system, with the previous finger pairs serving to shift larger particles into increasingly slower flow. In the case where the acoustic force varies across the length of the IDTs (as in Fig. 4b), this will occur in the region where the

acoustic force is at a maximum.

The separation enhancing effect that multiple acoustic nodes affords can be theoretically described as follows; as the particles pass through the pressure field they are displaced laterally in two ways. (1) a small shift each time an acoustic force maxima is crossed and (2) a larger shift across the width of the field when a particle is trapped in an acoustic node, when  $F_{aco}^{max} \geq F_D^{max}$ . The latter is critical for sorting, but the former also aids the process. If we combine the scaling of the drag and acoustic force and examine the ratio between them, we find that  $\tilde{F} \equiv F_{aco}/F_D \sim R^2/v$ . If we then define the ratio between two different particle size populations  $\alpha = R_{small}/R_{large}$  and the ratio of the fluid velocities that each particle population will experience at a given point in the  $x$ -direction,  $\beta = v_{small}/v_{large}$ , then it follows that

$$\frac{\tilde{F}_{large}}{\tilde{F}_{small}} \sim \frac{\beta}{\alpha^2}. \quad (10)$$

The larger this ratio, between the force on the larger and smaller particle populations, the better sorting will be. As expected, the relative force experienced between two different particle sizes scales with the square of ratio of the difference in particle sizes. Due to the lateral deflection occurring at each acoustic force maxima,  $\beta$  increases with the number of IDT finger pairs, enhancing the separation effect. This aids sorting due to small variation in the forces experienced by an individual particle due to interparticle forces, the effect of nearby particles on the acoustic field and Brownian motion. The effect of different  $\beta$  could be further optimized in future iterations of the vDLD device by increasing the velocity profile gradient. The role of multiple acoustic force maxima becomes essential for submicron particles which experience a high degree of Brownian motion.

The advantages of having a finite number of pressure antinodes produced by IDT finger pairs placed directly in the channel are a result of practical, as well as theoretical considerations. By integrating the IDTs directly in the path of particle migration the pressure field can be strictly defined within the boundaries of the chamber, avoiding attenuation losses compared to the case where the IDTs are placed outside of the chamber. Additional finger pairs, in addition to permitting sorting at greater maximum flow velocities for a given pressure amplitude (Fig. 6b), practically also result in larger substrate velocities, and therefore pressures, for a given A/C signal.

## Conclusions

We have developed a deterministic sorting system that can be applied to a wide variety of particle/cell sizes. Placing IDT finger-pairs directly in the channel maximizes the acous-

tic force that is experienced by the particles and allows sorting based on either acoustic or DEP forces, with the dominant force being simply determined by choosing the channel height. Though the higher channel dimensions of the acoustic-dominant vDLD has advantages from a throughput and ease of fabrication standpoint, the system is versatile as a result. It is possible to sort based on essentially any particle/cell parameter by choosing the dominant force; the acoustic force for mechanical properties and the DEP force for electrical properties.

More generally, SAW devices are uniquely applicable to microfluidic particle separation because: (1) they are planar and can be easily integrated with other microfluidic processes, (2) the wavelength of a typical SAW device (5-300  $\mu\text{m}$ ) is of the same order of most microfluidic systems and (3) the localization of energy at the surface results in efficient transfer of energy to a fluid placed on top, and have therefore found application in microfluidic applications as diverse as atomization<sup>37,38</sup>, mixing<sup>39</sup>, concentration<sup>40</sup>, pumping<sup>41</sup>, droplet production<sup>42</sup> and microcentrifugation<sup>43</sup>.

Here we have presented a further utilization, vDLD, which takes advantage of the high frequencies and corresponding length scales associated with SAW. With the ability to separate particle populations of arbitrary dimensions, we expect the vDLD system to be applied to any field or application where deterministic separation of particles or cells by their physical properties is required.

## Acknowledgements

Principle fabrication of the vDLD devices was performed at the Melbourne Center for Nanofabrication (MCN), the Victorian node of the Australian National Fabrication Facility (ANFF).

## References

- 1 E. Riera-Franco de Sarabia, J. A. Gallego-Juárez, G. Rodríguez-Corral, L. Elvira-Segura, and I. González-Gómez, *Ultrasonics* **38**, 642 (2000).
- 2 P. Tartaj, M. del Puerto Morales, S. Veintemillas-Verdaguer, T. González-Carreno, and C. J. Serna, *Journal of Physics D: Applied Physics* **36**, R182 (2003).
- 3 J. C. Giddings, F. J. Yang, and M. N. Myers, *Analytical Biochemistry* **81**, 395 (1977).
- 4 D. Di Carlo, *Lab Chip* **9**, 3038 (2009).
- 5 M. Yamada and M. Seki, *Lab on a Chip* **5**, 1233 (2005).
- 6 Y. Wang, Y. Zhao, and S. K. Cho, *Journal of Micromechanics and Microengineering* **17**, 2148 (2007).
- 7 N. Xia, T. P. Hunt, B. T. Mayers, E. Alsberg, G. M. White-

- sides, R. M. Westervelt, and D. E. Ingber, *Biomedical Microdevices* **8**, 299 (2006).
- 8 M. MacDonald, G. Spalding, K. Dholakia, et al., *Nature* **426**, 421 (2003).
- 9 P. R. Gascoyne and J. Vykoukal, *Electrophoresis* **23**, 1973 (2002).
- 10 S. Park, Y. Zhang, T.-H. Wang, and S. Yang, *Lab on a Chip* **11**, 2893 (2011).
- 11 M. Wiklund, C. Günther, R. Lemor, M. Jäger, G. Fuhr, and H. M. Hertz, *Lab on a Chip* **6**, 1537 (2006).
- 12 J. Shi, H. Huang, Z. Stratton, Y. Huang, and T. J. Huang, *Lab Chip* **9**, 3354 (2009).
- 13 F. Petersson, A. Nilsson, C. Holm, H. Jönsson, and T. Laurell, *Lab on a Chip* **5**, 20 (2005).
- 14 C.-F. Chou, R. H. Austin, O. Bakajin, J. O. Tegenfeldt, J. A. Castelino, S. S. Chan, E. C. Cox, H. Craighead, N. Darnton, T. Duke, et al., *Electrophoresis* **21**, 81 (2000).
- 15 L. R. Huang, P. Silberzan, J. O. Tegenfeldt, E. C. Cox, J. C. Sturm, R. H. Austin, and H. Craighead, *Physical review letters* **89**, 178301 (2002).
- 16 S. L. Levy and H. G. Craighead, *Chemical Society Reviews* **39**, 1133 (2010).
- 17 L. R. Huang, E. C. Cox, R. H. Austin, and J. C. Sturm, *Analytical chemistry* **75**, 6963 (2003).
- 18 J. Han, J. Fu, and R. B. Schoch, *Lab Chip* **8**, 23 (2007).
- 19 K. J. Morton, K. Loutharback, D. W. Inglis, O. K. Tsui, J. C. Sturm, S. Y. Chou, and R. H. Austin, *Proceedings of the National Academy of Sciences* **105**, 7434 (2008).
- 20 L. R. Huang, E. C. Cox, R. H. Austin, and J. C. Sturm, *Science* **304**, 987 (2004).
- 21 D. W. Inglis, J. A. Davis, R. H. Austin, and J. C. Sturm, *Lab on a Chip* **6**, 655 (2006).
- 22 J. A. Davis, D. W. Inglis, K. J. Morton, D. A. Lawrence, L. R. Huang, S. Y. Chou, J. C. Sturm, and R. H. Austin, *Proceedings of the National Academy of Sciences* **103**, 14779 (2006).
- 23 K. Loutharback, K. S. Chou, J. Newman, J. Puchalla, R. H. Austin, and J. C. Sturm, *Microfluidics and nanofluidics* **9**, 1143 (2010).
- 24 H. Morgan, A. G. Izquierdo, D. Bakewell, N. G. Green, and A. Ramos, *Journal of Physics D: Applied Physics* **34**, 1553 (2001).
- 25 C.-F. Chou, O. Bakajin, S. W. Turner, T. A. Duke, S. S. Chan, E. C. Cox, H. G. Craighead, and R. H. Austin, *Proceedings of the National Academy of Sciences* **96**, 13762 (1999).
- 26 L. Y. Yeo and J. R. Friend, *Biomicrofluidics* **3** (2009).
- 27 G. Destgeer, K. H. Lee, J. H. Jung, A. Alazzam, and H. J. Sung, *Lab on a Chip* **13**, 4210 (2013).
- 28 S. Shiokawa, Y. Matsui, and T. Ueda, in *Ultrasonics Symposium, 1989. Proceedings., IEEE 1989* (IEEE, 1989), pp. 643–646.
- 29 P. Tathireddy, Y.-H. Choi, and M. Skliar, *Journal of Electrostatics* **66**, 609 (2008).
- 30 Y. Chen, A. A. Nawaz, Y. Zhao, P.-H. Huang, J. P. McCoy, S. J. Levine, L. Wang, and T. J. Huang, *Lab on a Chip* (2014).
- 31 Y. Chen, S. Li, Y. Gu, P. Li, X. Ding, L. Wang, J. P. McCoy, S. J. Levine, and T. J. Huang, *Lab on a Chip* (2014).
- 32 Y. Chen, X. Ding, S.-C. Steven Lin, S. Yang, P.-H. Huang, N. Nama, Y. Zhao, A. A. Nawaz, F. Guo, W. Wang, et al., *ACS nano* **7**, 3306 (2013).
- 33 R. Tucoulou, M. Brunel, D. V. Roshchupkin, I. A. Schelokov, J. Colin, and J. Grilhe, *Ultrasonics, Ferroelectrics and Frequency Control, IEEE Transactions on* **46**, 856 (1999).
- 34 A. Holm, P. Wallner, W. Ruile, and R. Weigel, in *Ultrasonics Symposium, 1997. Proceedings., 1997 IEEE* (IEEE, 1997), vol. 1, pp. 153–156.
- 35 S. M. Langelier, L. Y. Yeo, and J. Friend, *Lab on a Chip* **12**, 2970 (2012).
- 36 H. Bruus, *Lab on a Chip* **12**, 1014 (2012).
- 37 D. Collins, O. Manor, A. Winkler, H. Schmidt, J. Friend, and L. Yeo, *Physical Review E* **86**, 056312 (2012).
- 38 J. Ju, Y. Yamagata, H. Ohmori, and T. Higuchi, *Sensors and Actuators A: Physical* **147**, 570 (2008).
- 39 R. Shilton, M. Tan, L. Yeo, and J. Friend, *Journal of Applied Physics* **104**, 014910 (2008).
- 40 J. Shi, X. Mao, D. Ahmed, A. Colletti, and T. Huang, *Lab on a Chip* **8**, 221 (2008).
- 41 M. Tan, L. Yeo, and J. Friend, *Europhysics Letters* **87**, 47003 (2009).
- 42 D. Collins, T. Alan, K. Helmerston, and A. Neild, *Lab Chip* (2013).
- 43 N. R. Glass, R. J. Shilton, P. P. Chan, J. R. Friend, and L. Y. Yeo, *small* **8**, 1881 (2012).